OPEN ACCESS
IOP Publishing
Journal of Physics B: Atomic, Molecular and Optical Physics
J. Phys. B: At. Mol. Opt. Phys. **57** (2024) 125001 (9pp)
https://doi.org/10.1088/1361-6455/ad421c

R-matrix calculations for opacities: I. Methodology and computations

A K Pradhan[1,2,3,*], **S N Nahar**[1] and **W Eissner**[4,†]

[1] Department of Astronomy The Ohio State University, Columbus, OH 43210, United States of America
[2] Biophysics Graduate Program The Ohio State University, Columbus, OH 43210, United States of America
[3] Chemical Physics Program, The Ohio State University, Columbus, OH 43210, United States of America
[4] Institüt für Theoretische Physik, Teilinstitut 1, 70550 Stuttgart, Germany

E-mail: pradhan.1@osu.edu

Received 23 August 2023, revised 28 February 2024
Accepted for publication 23 April 2024
Published 17 May 2024

Abstract

An extended version of the *R*-matrix methodology is presented for calculation of radiative parameters for improved plasma opacities. Contrast and comparisons with existing methods primarily relying on the distorted wave approximation are discussed to verify accuracy and resolve outstanding issues, particularly with reference to the opacity project (OP). Among the improvements incorporated are: (i) large-scale Breit–Pauli *R*-matrix calculations for complex atomic systems including fine structure, (ii) convergent close coupling wave function expansions for the (e + ion) system to compute oscillator strengths and photoionization cross sections, (iii) open and closed shell iron ions of interest in astrophysics and experiments, (iv) a treatment for plasma broadening of autoionizing resonances as function of energy-temperature-density dependent cross sections, (v) a 'top-up' procedure to compare convergence with *R*-matrix calculations for highly excited levels, and (vi) spectroscopic identification of resonances and bound (e + ion) levels. The present *R*-matrix monochromatic opacity spectra are fundamentally different from OP and lead to enhanced Rosseland and Planck mean opacities. An outline of the work reported in other papers in this series and those in progress is presented. Based on the present re-examination of the OP work, opacities of heavy elements might require revisions in high temperature-density plasma sources.

Keywords: *R*-matrix, opacities, plasma effects, astrophysics

1. Introduction

Opacity is due to interaction of radiation with matter. It is a fundamental parameter in plasma, astrophysics, and atomic physics that determines radiation transport, and entails absorption and scattering of photons by atoms at all frequencies of radiation prevalent in a given environment. Methods for calculating opacities are well-established, and essentially involve the atomic physics of bound-bound and bound-free transition probabilities incorporated within an equation-of-state (EOS) of the plasma [1–4]. However, in practice complexities arise owing to several physical factors that influence the accurate determination of opacity, and are addressed in this series of papers. As this work is an extension of the opacity project (hereafter OP), we first briefly outline OP and its calculations described under the *Atomic data for opacities* (hereafter ADOC) series of papers, and their limitations. Next, we describe the extensions and improvements over OP in the

† Deceased.
* Author to whom any correspondence should be addressed.

present series *R-Matrix calculations for opacities* (hereafter RMOP), subsequently referred to as papers RMOP1, RMOP2, RMOP3, RMOP4.

1.1. The OP

The OP work by Seaton and collaborators ([1–3] and references therein) was devoted to the development of a framework for calculation of opacities based on the close coupling approximation implemented in the powerful *R*-matrix (RM) method by Burke and collaborators, and employed extensively for accurate calculations of a variety of radiative and collisional atomic processes [5–7]. The OP work entailed an EOS for stellar interior plasmas based on the 'chemical picture' by Mihalas, Hummer and Däppen (named MHD-EOS [8]), that connects physically with OP atomic data via an *occupation probability* factor of ionization fractions, level populations, and partition function in the modified Saha–Boltzmann equations that accounts for plasma interactions.

Despite unprecedented effort and advances, the OP *R*-matrix work reported in ADOC faced several then intractable difficulties that limited the scope of atomic calculations. Primarily, the limitations were due to computational constraints which, in turn, did not enable accounting for important physical effects and a complete *R*-matrix calculation of atomic opacities. The main features and deficiencies of OP are as follows: (I) the calculations were in LS coupling neglecting relativistic fine structure, (II) the close coupling (hereafter CC) wavefunction expansion for the target or the core ion in the (e + ion) system included only a few ground configuration LS terms, (III) inner-shell excitations could not be included owing to the restricted target ion expansion, (IV) while autoionizing resonances in bound-free photoionization cross sections were delineated within the few excited target terms, (V) total angular and spin (e + ion) symmetries with large orbital angular-spin quantum numbers were not computed. All of these factors are crucial for a complete and accurate opacity calculation. Therefore, the OP work incorporated a relatively small subset of *R*-matrix data. Rather, most of the opacities contributions were obtained using atomic structure codes and the distorted wave (hereafter DW) approximation, similar to other opacity models [7–11].

In addition to the limitations of ADOC work mentioned above, new physical issues emerge in extending *R*-matrix calculations towards a complete calculation of opacities. There are three major problems that need to be solved: (A) convergence of large coupled channel wavefunction expansions necessary to include sufficient atomic structures manifest in opacity spectra, (B) completeness of high $n\ell$ contributions up to $n \equiv \infty$, and (C) attenuation of resonance profiles due to *intrinsic* autoionization broadening (included in RM calculations in an *ab initio* manner) and *extrinsic* plasma effects due to temperature and density, as generally considered for bound-bound line opacity.

1.2. Scientific problems

The erstwhile OP work summarized above concluded that the agreement between OP and another independent calculation OPAL [3, 12] do not differ by more than 2.5%, implying that a further revision of opacities was not needed [13]. However, there are outstanding problems related to opacities derived from the OP and all other opacity models. The foremost among them is related to a downward revision of solar abundances of common volatile elements such as carbon, nitrogen, oxygen and neon, relative to earlier ones by up to ∼50% [14, 15]. Thereupon, astrophysicists suggested that an *upward* revision of opacities by ∼10% [16, 17] would countenance the lower solar abundances, since abundances are inversely linked to opacities which affect the radiation field in non-local thermodynamic equilibrium models employed to analyze observed line profiles of elements. In particular, the iron opacity plays a crucial role owing to relatively high abundance of iron. Also, recent experimental measurements of iron opacity were higher than given by OP and other models [19, 20]. Whereas opacity models have been improved by including additional transition arrays resonances, etc the discrepancies with astrophysical and experimental results remain outstanding.

This series describes the work carried out since the OP opacities reported in 2003 and available via database OPServer [21].

1.3. Breit–Pauli R-matrix (BPRM) and DW methods

Current opacity models employ the DW approximation or variants thereof ([22] and references therein). In order to compare and contrast the present BPRM results, as well as to test complementarity and completeness of atomic data, we have also carried out relativistic DW calculations reported in paper RMOP3 of this RMOP series. In principle, the DW approximation based on an atomic structure calculation coupled to the continuum yields complete sets of opacities. Oscillator strengths and photoionization cross sections are computed for all possible bound-bound and bound-free transitions among levels specified by electronic configurations included in the atomic calculation (viz. [23], see RMOP4). However, since the DW approximation includes only the coupling between initial and final states, the complexity of interference between the bound and continuum wavefunction expansions involving other levels is neglected [18]. That manifests itself as quasi-bound levels and autoionizing resonances embedded in the continua. DW models employ the independent resonance approximation that treats the bound-bound transition probability independently from coupling to the continuum [7]. Apart from relative simplicity of atomic computations, the advantages of DW models is that well-established line broadening treatments may be employed to account for plasma interactions [24]. Another advantage is ease of completeness of datasets that can be augmented

by including additional configurations with multiple-electron excitations (see RMOP4). Furthermore, high angular-spin momenta do not pose a computational problem commonly encountered in CC calculations. For these reasons the DW method is generally employed for opacities calculations. In contrast, RMOP calculations are computationally laborious and time-consuming; however, coupling effects can affect atomic parameters significantly, as demonstrated in RMOP2 and RMOP4.

1.4. Prior work

Opacity in the bound-free continuum is dominated by autoionizing resonances, as shown in recently completed works cited above and present results. Hitherto, they have been treated generally as lines akin to bound-bound transitions. The most important consequence, and likely source of missing opacity, is the *intrinsic* autoionizing broadening and the *extrinsic* plasma broadening thereof. The much wider spread of resonances in the continuum than lines raises the opacity significantly [4, 25, 26].

Recent work [24] (hereafter D21) extended Fe XVII *R*-matrix calculations by including more configurations than [25] (hereafter NP16). Whereas that confirmed our earlier results for photoionization cross sections, there are several issues: (i) do not consider plasma broadening of autoionizing resonances that enhance opacities significantly, (see papers II and III), (ii) the D21 comparison between DW and unbroadened RM appears to agree, although fundamentally different since the DW method treats autoionizing levels and broadening thereof as for lines, (iii) D21 do not compare unbroadened RM cross sections for Fe XVII previously available from database NORAD [27], (iv) inexplicably, the D21 RM Fe XVII Rosseland mean opacities are 10% below the primarily DW results from OP (available from OP database TOPbase [28], see also [21]), whereas all other DW models yield values up to 1.5 times higher [26]. There is no reason why RM opacities, even without broadening, should be lower than OP and other DW models, except that D21 might have an incomplete number of bound Fe XVII levels in their RM calculations. Other issues such as radiative data, cross sections, and shapes of autoionizing resonances due to plasma broadening are addressed in this RMOP series.

Experimental opacity measurements at the Sandia Z facility for Fe, Ni, and Cr have highlighted deficiencies in theoretical models [19, 20]. However, experimental results need to be viewed in the context of the *very limited energy range where monochromatic iron opacity is actually measured*. Indeed, the experimental energy range does *not* include the region of maximum opacity from Fe ions around ∼1 KeV (well-known in x-ray spectroscopy). Therefore, experimental opacities *per se* contribute only about 20% to the Rosseland mean opacities directly. However, extrapolating the differences between OP and experimental data in that limited range, B15 estimate a solar mixture opacity enhancement of $7 \pm 3\%$ (the large error bars imply a factor of 2.5 discrepancy between the low and high experimental values).

Opacity is a sensitive function of temperature and density, and an incomplete tabulation in a limited range may give inconsistent results since different ionization states of Cr, Fe and Ni contribute. For example, N-like Cr ions with 3 active p-electrons make the largest contribution at the Z temperature/density, whereas F-like Fe with 5 p-electrons is the largest contributor; for Ni it is Ne-like, a closed p-shell configuration. These issues need to be examined individually at a much wider range of energy-temperature-density to ascertain the source of discrepancies. Thus, although experimental results might point to 'missing physics', it is first important to include physics that is known but missing, such as plasma broadening described in this series of Papers.

1.5. Overview of RMOP calculations

Sections of this first paper RMOP1 cover the following topics, as well as general features of subsequent papers in the series: (i) opacities and solar temperature-density structure, (ii) local-thermodynamic-equilibrium (LTE) plasma EOS valid in stellar interiors, (iii) relativistic effects using the BPRM approximations, (iv) DW and BPRM calculations, and (v) plasma broadening of autoionizing resonances in bound-free opacity, (vi) convergence and completeness of atomic data.

2. Monochromatic and mean opacities

The atomic parameters comprising the monochromatic opacity are due to bound-bound (bb), bound-free (bf), free-free (ff), and photon scattering (sc) contributions:

$$\kappa_{ijk}(\nu) = \sum_k a_k \sum_j x_j \sum_{i,i'} \left[\kappa_{bb(}(i,i';\nu) + \kappa_{bf}(i,\epsilon i';\nu) + \kappa_{ff}(\epsilon i,\epsilon' i';\nu) + \kappa_{sc}(\nu)\right] , \quad (1)$$

where a_k is the abundance of element k, x_j the j ionization fraction, i and i' are the initial bound and final bound/continuum states of the atomic species, and ϵ represents the electron energy in the continuum. The atomic absorption coefficients are related to the local radiation field at temperature T described by the Planck function

$$B_\nu(T) = \frac{\left(2h\nu^3/c^2\right)}{e^{h\nu/kT} - 1}. \quad (2)$$

Macroscopic quantities such as radiative forces and fluxes may be computed in terms of mean opacities, such as the Planck mean opacity

$$\kappa_P B(T) = \int \kappa_\nu B_\nu \mathrm{d}\nu. \quad (3)$$

Of particular interest to opacity calculations is the Rosseland mean opacity (RMO), κ_R RMO defined as the *harmonic mean* of monochromatic opacity $\kappa_{ijk}(\nu)$ as

$$\frac{1}{\kappa_R} = \frac{\int_0^\infty g(u)\,\kappa_\nu^{-1}\mathrm{d}u}{\int_0^\infty g(u)\,\mathrm{d}u} \quad ; \quad g(u) = u^4 e^{-u}\left(1 - e^{-u}\right)^{-2}, \quad (4)$$

Table 1. Solar opacity parameters derived from [31] using elemental abundances from [14, 15] (numbers in parenthesis are powers of 10), with the exception of the central temperature at $r/R_\odot = 0$ from several other sources. The boundary of the radiative zone and BCZ is accurately determined from helioseismology to be 0.713 ± 0.001 [32, 33].

$r/R_\odot$	ρ (g cc^{-1})	T (K)	N_e (cm^{-3})
0.00	162.2	1.58(7)	1.0(26)
0.35	6.89	5.75(6)	3.57(24)
0.40	3.88	5.01(6)	2.01(24)
0.45	2.29	4.47(6)	1.19(24)
0.50	1.31	3.89(6)	6.82(23)
0.55	0.82	3.47(6)	4.25(23)
0.60	0.51	3.09(6)	2.67(23)
0.65	0.33	2.69(6)	1.71(23)
0.71	0.20	2.24(6)	1.02(23)

Table 2. Main solar BCZ atomic opacity contributing elements and ionization states and fractions >0.03, at $T = 2.24 \times 10^6$ K and $N_e = 10^{23}$ cm^{-3}, obtained from [34] using the Q-form of the MHD-EOS [8, 9]. The actual elemental opacity contributions depend significantly on the theoretical model employed with respect to solar abundances and the EOS [4, 35].

Element	Ionization state (fraction)
Oxygen	O VII (0.11), O VIII (0.47), O IX (0.42)
Neon	Ne VIII (0.10), Ne IX (0.51), Ne X (0.35)
Iron	Fe XVI (0.031), Fe XVII (0.196), Fe XVIII (0.372), Fe XIX(0.284), Fe XX (0.098)

where $g(u) = \mathrm{d}B_\nu/\mathrm{d}T$ is the derivative of the Planck weighting function (corrected for stimulated emission). Equation (4) is mathematically and physically a complex quantity to evaluate. Whereas the opacity determines radiative transfer through the stellar interior, the RMO is related to the total radiation flux that eventually escapes the star and observed [29]. Although the singularity in the denominator $1/\kappa_n u$ is generally avoided owing to overlapping spectral features, the RMO depends critically on the precise distribution of monochromatic opacity at all frequencies at a given **temperature T (K) and matter density ρ (g cc^{-1})** at each point inside the star. The opacity spectrum is a complex quantity with superimposed dips or windows and large peaks that vary by orders of magnitude due to energy dependence of atomic parameters, $\kappa_{bb}(i,i') = (\pi e^2/m_e c) N_i f_{ii'} \phi_\nu$, and $\kappa_{bf} = N_i \sigma_\nu$. The κ_ν is then primarily a function of the bb oscillator strengths f, bf photoionization cross sections σ_ν, level populations N_i, and the line-profile factor ϕ_ν. The RMOP framework for large-scale computations comprises mainly the first two components of the opacity in equation (1): (i) the bb transition probabilities and (ii) the bf photoionization cross sections.

2.1. Solar structure and opacity

Tables 1 and 2 provide a numerical glimpse of solar interior structure and related plasma and atomic parameters [1, 3, 7, 22]. In table 1 we focus on the region outside of the nuclear fusion core in the radiative zone up to the boundary at the base of the convection zone (BCZ) [30]. Helioseismological analysis of thousands of modes of solar oscillations yields a precise measurement of the BCZ at solar radius $\mathrm{R}_\odot = 0.713 \pm 0.001$. At and above the BCZ outward energy transport via radiative diffusion gives way to convection which becomes more efficient since $(\mathrm{d}T/\mathrm{d}r)_{\rm diff} > (\mathrm{d}T/\mathrm{d}r)_{ad}$, the adiabatic temperature gradient. There are two main reasons for convective motions to be more efficient at the BCZ: the weight of the outer layers is less than the radiation pressure from the interior below, and the *increase* in opacity from higher to lower temperatures. Opacity increases due to the prevalence of lower stages of ionization, as more bound electrons are active in absorption of radiation via larger number of bound-bound and bound-free transitions than at higher temperatures below the BCZ.

Table 2 shows the ionization states of the dominant elements that determine opacity at the BCZ: O, Ne and Fe [4, 19]. Almost 90% oxygen is in H-like or fully ionized [4], and 86% of neon is in H-like and He-like ionization states. But one and two electron K-shell ionization states do not contribute as much to opacity, as lower ones such as the partially filled L-shell Fe ions with percentage contributions given in table 2. Just three Fe ions constitute 85% of iron at BCZ temperatures and densities. Those ions, Fe XVII, XVIII, XIX have very complex atomic structure and large number of radiative transitions that need to be accounted for. Large-scale calculations are necessary to compute accurate opacities, and detailed calculations for these three ions are reported in RMOP2.

In table 3 we present a sample of the lowest and highest levels for the Fe XVIII that has the highest ionization fraction of all Fe ions at BCZ conditions (table 2). As described in paper RMOP2, RMOP calculations for Fe XVIII yield 1174 bound levels, and a total of 1604 levels including high-lying levels with $n > 4$ described in paper RMOP4 calculations to test convergence and completeness. The MHD-EOS parameters given in table 3 demonstrate the typical distribution of occupation probabilities and level populations across the bound-level spectrum of complex Fe ions. Very high-lying

Table 3. MHD equation-of-state at the temeprature T(K) and electron number density N_e (per cubic centimeter) parameters for Fe XVIII at solar BCZ: $T = 2 \times 10^6$ K, $N_e = 10^{23}$ cc^{-1}. Out of 1604 bound levels calculated, the lowest six levels, energies, occupation probabilities W(OP), and percentage level populations are given. The highest bound levels approaching the first ionization threshold $E \to 0$ are also given. The rapid decrease in W and N(%pop) by orders of magnitude is evident. Notation: $4.06(-5) = 4.06 \times 10^{-5}$.

Level	Energy (Ry)	W(OP)	N(% pop)
$1s^2 2s^2 2p^5 (^2P^o_{3/2})$	−99.924	1.00	8.79
$1s^2 2s^2 2p^5 (^2P^o_{1/2})$	−99.010	1.00	4.09
$1s^2 2s^2 2s (^1S_0)$	−90.156	1.00	2.03
$1s^2 2s^2 2p^4 3s (^4P_{5/2})$	−43.203	0.99	0.15
$1s^2 2s^2 2p^4 3s (^4P_{3/2})$	−42.957	0.99	0.05
$1s^2 2s^2 2p^4 3s (^4P_{1/2})$	−42.477	0.99	0.05
Highest levels $n > 4$	−0.500	0.56	4.06(−5)
Non-hydrogenic	−0.343	0.01	1.10(−7)

levels make insignificant contribution to opacity calculations. Previous works have discussed the inexplicable differences of orders of magnitude in occupation probabilities between OP and OPAL [36]. The EOS issue therefore remains open for future study [4].

2.2. LTE EOS

Stellar interiors are generally assumed to be characterized by a local temperature-density (TD) parameter in LTE at any given point in the star. However, TD tracks vary by orders of magnitude as nuclear energy produced in the core is transported through the radiative diffusion zone and the materially convective zones up to the atmosphere where radiation escapes. A realistic EOS must therefore account for atomic-plasma effects all throughout. In the first paper on OP opacities ([2], hereafter SYMP), the authors defined 'stellar envelopes to be regions where atoms are not markedly perturbed by the plasma environment'; the stellar envelope generally comprising of radiative and convection zones.

The MHD-EOS is a modified version of the Saha–Boltzmann equations, based on the concept of *occupation probability* w of an atomic level being populated, taking into account perturbations of energy levels by the plasma environment,

$$N_{ij} = \frac{N_j g_{ij} w_{ij} e^{-E_{ij}/kT}}{U_j}. \tag{5}$$

The w_{ij} are the occupation probabilities of levels i in ionization state j. The occupation probabilities do not have a sharp cut-off, but approach zero for high-n as they are 'dissolved' due to plasma interactions. The partition function is re-defined as

$$U_j = \sum_i g_{ij} w_{ij} e^{(-E_{ij}/kT)}. \tag{6}$$

E_{ij} is the excitation energy of level i, g_{ij} its statistical weight, and T the temperature. The w_{ij} are determined upon free-energy minimization in the plasma at a given temperature-density. An atomic level i is considered dissolved by the plasma microfield when its highest Stark sub-level overlaps with the lowest sub-level of the $i+1$ level (discussed further in RMOP3).

The original version of MHD-EOS estimated the range of validity to $\rho < 0.02$ g cc^{-1} [8]. That rather restrictive density limit is less than prevalent at the BCZ (cf table 1), and most of the solar interior. The later version called the Q-MHD [9] has been employed in all present calculations. However, the EOS employed by OPAL differs considerably from OP; these differences and approximations made in the OP work, have been previously discussed, particularly for H-like ions for which data have been available [3, 36]. Nevertheless, the agreement between OP and OPAL to <5% [18] seems to indicate that the differences in EOS do not affect final results. But the EOS redistributes level populations significantly; further work on improving the MHD-EOS is in progress.

3. *R*-matrix opacity calculations

In this section we describe in some detail the differences from the OP work mentioned previously. In addition, a description of the revised RMOP codes, related extensions, and the new set of opacity codes is described.

3.1. Convergent close coupling calculations

Owing to the fact that the OP R-matrix calculations included only a few LS terms of the target or core ion, the (e + ion) wavefunction expansions were far from convergence of computed quantities and completeness. In the present work, particularly for iron ions reported in RMOP2, an effort is made to ensure convergence of photoionization calculations in the close coupling (CC) approximation using the R-matrix method as developed in the OP [3], and later in the iron project (IP) [11]. In the CC approximation, the atomic system is represented as the 'target' or the 'core' ion of N-electrons interacting with the $(N+1)$th electron. The $(N+1)$th electron may be bound in the electron-ion system, or in the electron-ion continuum depending on its energy to be negative or positive. The total wavefunction, Ψ_E, of the $(N+1)$-electron system in a symmetry $SL\pi$ or $J\pi$ is an expansion over the eigenfunctions of the target ion, χ_i in specific state $S_i L_i (J_i) \pi_i$, coupled with the $(N+1)$th electron function, θ_i:

$$\Psi_E (e + \text{ion}) = A \sum_i \chi_i (\text{ion})\, \theta_i + \sum_j c_j \Phi_j, \tag{7}$$

where the sum is over the ground and excited states of the target or the core ion. The $(N+1)$th electron with kinetic energy k_i^2 corresponds to a channel labeled $S_i L_i (J_i) \pi_i k_i^2 \ell_i (SL(J)\pi)$. The Φ_js are bound channel functions of the $(N+1)$-electron system that account for short range correlation not considered

in the first term and the orthogonality between the continuum and the bound electron orbitals of the target.

Substitution of $\Psi_E(e+\text{ion})$ in the Schrodinger equation

$$H_{N+1}\Psi_E = E\Psi_E \tag{8}$$

introduces a set of coupled equations that are solved using the *R*-matrix method. The solution is a continuum wavefunction Ψ_F for an electron with positive energies ($E > 0$), or a bound state Ψ_B at a *negative* total energy ($E \leqslant 0$). The complex resonance structures in photoionization cross sections result from channel couplings between the continuum channels that are open ($k_i^2 > 0$), and ones that are closed ($k_i^2 < 0$). Resonances occur at electron energies k_i^2 corresponding to autoionizing states belonging to Rydberg series, $S_iL_i\pi_i\nu\ell$ where ν is the effective quantum number, converging on to the target threshold S_iL_I.

Convergence of the (e + ion) expansion in equation (1) is a difficult computational problem in CC calculations, since the numerical size of the Hamiltonian increases as square of the total number of channels in both the first and the second sum on the RHS. For example, the calculations reported in RMOP2 there are hundreds of target levels for each iron ion and thousands of corresponding channels. In general, for simpler atomic systems than considered herein it is preferable to substitute measured target level energies from available sources [37] for improved accuracy. However, given the several hundred target levels for the complex iron ions with multitude of overlapping resonances structures converging on to those, and missing experimental data for some levels, we employ calculated target energies that are in fact quite close to experimental values and result in insignificant effect on opacity calculations (discussed further in RMOP2).

3.2. Relativistic effects and BPRM codes

The limited OP *R*-matrix calculations did not consider fine structure. However, subsequent IP work employed the BPRM framework [11, 38] including fine structure target levels and recoupling scheme LS $\rightarrow$ LSJ. The relativistic BPRM Hamiltonian is given by

$$H_{N+1}^{\rm BP} = \sum_{i=1}^{N+1}\left\{-\nabla_i^2 - \frac{2Z}{r_i} + \sum_{j>i}^{N+1}\frac{2}{r_{ij}}\right\} + H_{N+1}^{\rm mass} + H_{N+1}^{\rm Dar} + H_{N+1}^{\rm so}, \tag{9}$$

where the last three terms are relativistic corrections:

$$\begin{aligned}&\text{the mass correction term, } H^{\rm mass} = -\tfrac{\alpha^2}{4}\textstyle\sum_i p_i^4,\\ &\text{the Darwin term, } H^{\rm Dar} = \tfrac{Z\alpha^2}{4}\textstyle\sum_i \nabla^2\left(\frac{1}{r_i}\right),\\ &\text{the spin}-\text{orbit interaction term, } H^{\rm so} = Z\alpha^2\textstyle\sum_i \frac{1}{r_i^3}\mathbf{l_i}.\mathbf{s_i},\end{aligned} \tag{10}$$

respectively.

The BPRM codes used for the present opacity calculations are shown in figure 1, which is modified from the LS coupling version given in ADOC II [6, 7, 39]. The atomic structure codes Superstructure (SS), CIV3, STG1, STG2, STGH, STGB, STGF, STGBB and STGBF are described in [6]. Briefly, SS and CIV3 are atomic structure codes; either one is first employed to obtain reasonably accurate target wavefunctions, eigenenergies, and oscillator strengths for the target ion. The target ion orbital radial functions are then used by STG1 to reconstruct the target and calculate *R*-matrix basis functions and radial integrals for the (e + ion) system. With radial integrals from STG1 as input, STG2 computes angular coefficients and matrices of the Hamiltonian and dipole operators. The BP recoupling LS $\rightarrow$ LSJ is implemented in the code RECUPD [38]. STGH diagonalizes the BP Hamilitonian and produces the H and D files required to obtain physical parameters such as energy levels and radiative data such as oscillator strengths and photoionization cross sections.

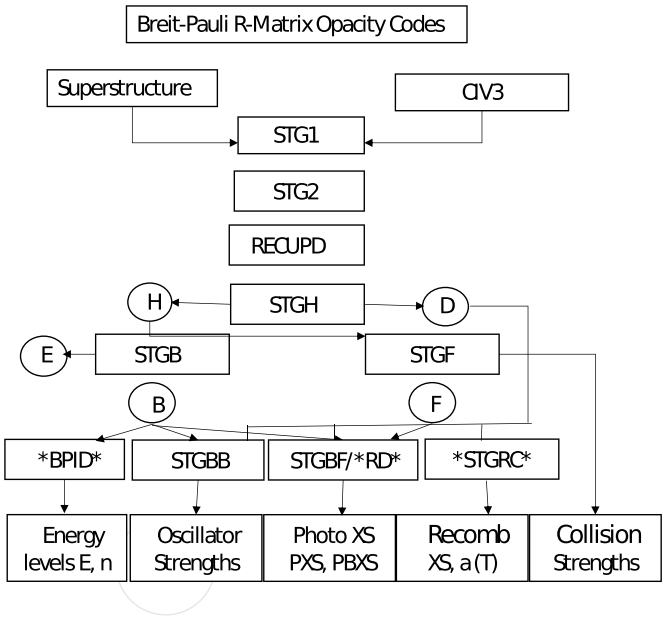

Figure 1. *R*-matrix codes for opacity calculations.

Other new codes or extended versions (bracketed by asterisks) comprise of the following.

3.3. Level identification

Energy levels from *R*-matrix calculations in STGB are obtained as eigenvalues of bound states of total angular momenta and parity $J\pi$, but without configuration and spin-angular designations, unlike atomic structure calculations where configurations are specified *a priori* and levels thereby identified. The new code BPID is employed to assign spectroscopic identification of all computed fine structure levels. Following diagonalization of the Hamiltonian matrix, the *R*-matrix basis functions are obtained and used to compute energy levels in STGB. BPID then analyzes the parameters computed in STGB to determine spectroscopic identification. Those are the channel percentage weights and quantum defects, complemented independently by atomic structure calculations. Level identification is necessary not only for spectroscopic designations required in practical applications, but also for matching and high $n\ell$(SLJ) 'top-up' of computed

oscillator strengths from STGBB and photoionization cross sections from STGBF to test completeness of atomic data.

3.4. Radiation damping

For highly charged ions, in particular H-like and He-like ions of Fe-group elements, radiative damping of autoionizing resonances is important (e.g. [40]), and may be considered using the extended code STGBF-RD. However, for opacities calculations this is not needed since total photon absorption cross section regardless of subsequent radiative decays is required.

3.5. Unified (e + ion) recombination

Level-specific and total (e + ion) recombination cross sections may be computed employing the unified method subsuming both radiative and di-electronic recombination in *ab initio* manner within the R-matrix CC formulation [41], using the code STGRC ([7], and references therein).

3.6. Convergence and completeness

In prior works such as NP16 [22, 25, 26], CC calculations employing target configurations and levels up to $n \leqslant 4$ are shown to 'converge' to practically acceptable accuracy in photoionization cross sections, as demonstrated in RMOP2 and RMOP4. Owing to the large number target levels considered the problem of pseudoresonances, sometimes encountered in more limited target expansions, is not encountered. That is because the correspondingly large number of closed channels in equation (7) accounts for the otherwise missing flux that might appear as pseudoresonances from bound channel correlation functions Φ_j in equation (7). However, since higher levels $n > 4$ are not included, completeness may not have been achieved with respect to all of the bound-bound and bound-free transitions and resulting opacity for a given ion. But R-matrix calculations become computationally intensive with increasing energy as successive thresholds of the target ion are exceeded and more channels open up. At the same time computations need to be done at all energies with a sufficiently fine energy mesh to resolve autoionization resonance structures. However, above the highest target level all channels are open and there are no more resonances. Although the number of open channels may be large, the cross sections are featureless and slowly varying with energy. Moreover, for high $n\ell$(SLJ) levels resonance structure are weak and may be neglected. In such cases a 'top-up' procedure using DW methods may be employed to test if convergence has been achieved to ensure completeness of atomic data for opacities. One such 'top-up' procedure is described in paper RMOP4. Generally, we find that the 'top-up' contribution to opacities is small and does not exceed ∼5% for any given ion.

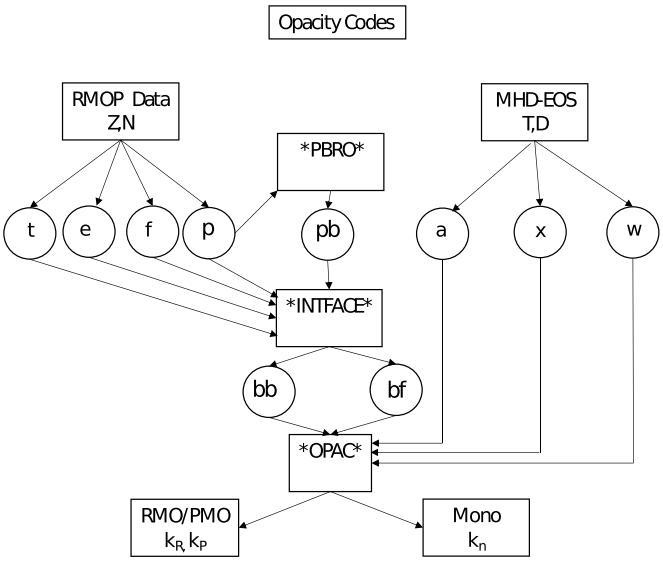

Figure 2. Plasma opacity codes.

3.7. Plasma effects

The OP and RMOP calculations are carried out for isolated atomic systems. As such, external effects due to plasma environment at specific temperature, density, abundances, etc need to be considered in opacity calculations. Those effects determine the EOS as discussed above. But in addition, they alter computed atomic features such as line shapes from bound-bound atomic transitions significantly (a discussion of the well-studied line profiles of H-like ions and approximations employed in OP work is given in [3, 42].

In OP work quasi-bound levels that give rise to resonances in the continuum are treated as bound levels *a priori*, and plasma broadening of autoionizing resonances is neglected due to, (i) difficulty in including pressure broadening, and (ii) because quantum interference between resonances and the continuum is considered to be small [36]. Therefore, a perturbative approach in the independent resonance approximation, akin to independent treatment of radiative and di-electronic recombination, is employed. However, as we demonstrate in Paper RMOP3 in detail, plasma broadening of autoionizing resonances fundamentally different from that of line broadening of bound levels. Practically, plasma broadening not only has a significant but large effect on bound-free opacity and derivative quantities such as the Rosseland and Planck mean opacities.

3.8. Opacities calculations

The opacity codes employed in RMOP calculations have not heretofore been published, and are different from those in the OP work. In the initial stages of OP, both sets of codes have been extensively checked against each other for opacities reported in [2]. However, most of OP data was from sources other than R-matrix calculations and processed to compute opacities in a different manner than described herein. Figure 2

shows the schematic diagram of the codes and datasets in RMOP calculations (codes bracketed by '∗' have not been heretofore presented).

3.8.1. Atomic data. The input RMOP data for opacity calculations are the final products from codes shown in figure 1. Each ion is treated as an (e + ion) system characterized by (Z,N), the atomic number Z and the number of electrons in the target ion.

The input atomic datasets consists of four files: (i) t-file—target level energies and statistical weights, (ii) e-file—energy levels as computed by STGB and further processes using BPID, (iii) f-file—oscillator strengths for E1 transitions computed in STGBB, (iv) p-file—photoionization cross sections from STGBF. These files are input to the code INTFACE that interfaces the atomic data, and maps out at a photon frequency mesh of 100 000 frequencies (in contrast the OP work is at 10 000 frequencies), into bound-bound (bb) and bound-free (bf) files for opacity calculations separately for each ion. *Prior to input into INTFACE, the p-files are pre-processed by the code PBRO for plasma broadening of autoionizing resonances in photoionization cross sections to produce broadened bf-files.* PBRO computes plasma broadened cross sections (described in RMOP3) for each temperature and density. This results in a large number of pb-files for all TD pairs from a single unbroadened p-file for each level of each ion of each element in opacities calculations. INTFACE then processes either the unbroadened p-files or broadened pb-files and produces corresponding bf-files mapped on to the opacity frequency mesh. Thus, a huge amount of data is produced as result of the interface of atomic and plasma parameters, most of it too large to be stored and therefore treated as intermediate files that are recreated for each TD.

3.8.2. EOS. The MHD-EOS parameters are taken from OPCD codes using the Q-form [3, 8, 9], so that there are no inconsistencies owing to the EOS between RMOP and OP. The input EOS parameters consist of: a—abundances of elements, x—ionization fractions of each ion, and w—EOS data to obtain occupation probabilities. The opacity code OPAC computes monochromatic, Planck and Rosseland mean opacities, $\kappa_\nu, \kappa_P, \kappa_R$ respectively, using the INTFACE bb and bf files, and EOS parameters, independently for each T-D, or ranges thereof. Since one of the primary motivation of the RMOP calculations is to solve the aforementioned solar abundances problem, different sets of abundances may be used to ascertain differences among them.

3.8.3. Bound and continuum opacities. The most important difference between RMOP and other opacity calculations is the treatment of bound-bound as distinct from bound-free continuum opacity. There is a clear division between lines as strictly the transitions among negative energy bound levels, and autoionizing resonances in the bound-free continua. Practically, this difference manifests itself in the code OPAC (figure 2). The bb-opacity consists of negative energy bound levels only, and corresponding oscillator strengths, and the bound-free opacity consists of photoionization cross sections with resonances that are otherwise treated as lines in DW opacity calculations. The DW calculations may couple lines *a posteori* to single-channel feature-less continuum perturbatively, but not in a fully coupled manner as in RMOP opacities. The combined bb and bf opacity spectra therefore are quite different in detail, which reflects in the calculation of mean opacities.

There are additional steps necessary in order to ensure completeness, as discussed in RMOP4, relating to the division between negative and positive energy levels and to ensure that there is no double-counting of levels if it is necessary to include high-$n\ell$ contributions, although they are found to matter little since high-lying levels have insignificant populations.

The treatment of free-free contribution to plasma broadening, discussed in RMOP3, is also implemented in OPAC. Large datasets of f-values for transitions *among positive energy levels*, obtained from atomic structure codes such as Superstructure or variants, are required to compute this contribution. Although, small relative to electron impact, Stark and Doppler broadening, it nevertheless needs to be included for completeness.

Based on the work described in this RMOP series, new iron opacities have been computed and compared with the OP work [4].

Data availability statement

The data that support the findings of this study will be openly available following an embargo at the following URL/DOI: https://norad.astronomy.osu.edu/.

Acknowledgments

This work has been partially supported by grants from the US National Science Foundation, NASA, and the Department of Energy. Most of the computational work was carried out at the Ohio Supercomputer Center.

ORCID iDs

A K Pradhan https://orcid.org/0000-0001-8775-3643
S N Nahar https://orcid.org/0000-0002-8750-3836

References

[1] Seaton M J 1987 *J. Phys. B: At. Mol. Phys.* **20** 6363
[2] Seaton M J, Yu Y, Mihalas D and Pradhan A K 1994 *Mon. Not. R. Astron. Soc.* **266** 805
[3] 1995 *The Opacity Project Team, The Opacity Project* vol 1 (IOP Publishing)
[4] Pradhan A K 2024 *Mon. Not. R. Astron. Soc.* **527** L179
[5] Burke P G 2011 *R-Matrix Theory of Atomic Collisions* (Springer)
[6] Berrington K A, Burke P G, Butler K, Seaton M J, Storey P J, Taylor K T and Yan Y 1987 *J. Phys. B: At. Mol. Phys.* **20** 6379
[7] Pradhan A K and Nahar S N 2011 *Atomic Astrophysics and Spectroscopy* (Cambridge University Press)

[8] Mihalas D, Hummer D G and Däppen W 1988 *Astrophys. J.* **331** 815
[9] Nayfonov A, Däppen W, Hummer D G and Mihalas D 1999 *Astrophys. J.* **526** 451
[10] Eissner W, Jones M and Nussbaumer H 1974 *Comput. Phys. Commun.* **8** 270
[11] Hummer D G, Berrington K A, Eissner W, Pradhan A K, Saraph H E and Tully J A 1993 *Astron. Astrophys.* **279** 298
[12] Rogers F J and Iglesias C A 1991 *Astrophys. J. Supp. Ser.* **79** 507 Ibid. [3]
[13] Badnell N R *et al* 2005 *Mon. Not. R. Astron. Soc.* **360** 458
[14] Asplund M, Grevesse N, Sauval A J and Scott P 2009 *Annu. Rev. Astron. Astrophys.* **47** 481
[15] Asplund M, Amarsi A M and Grevesse N 2021 *Astron. Astrophys.* **653** A141
[16] Bahcall J N, Pinsonneault M H, Basu S and Serenelli A M 2005 *Astrophys. J.* **618** 1049
[17] Basu S and Antia H M 2004 *Astrophys. J.* **606** L85
[18] Seaton M J and Badnell N R 2004 *Mon. Not. R. Astron. Soc.* **354** 457
[19] Bailey J E *et al* 2015 *Nature* **517** 56
[20] Nagayama T *et al* 2019 *Phys. Rev. Lett.* **122** 235001
[21] Mendoza C, Seaton M J, Buerger P, Bellorin A, Melendez M, Gonzalez J, Rodriguez L S, Palacios E, Pradhan A K and Zeippen C J 2007 *Mon. Not. R. Astron. Soc.* **378** 1031
[22] 2018 *Workshop on Astrophysical Opacities* (*ASP Conf. Ser.* vol 515)
[23] Gu M F 2008 *Can. J. Phys.* **86** 675
[24] Delahaye F D, Ballance C P, Smyth R T and Badnell N R 2021 *Mon. Not. R. Astron. Soc.* **508** 421
[25] Nahar S N and Pradhan A K 2016 *Phys. Rev. Lett.* **116** 235003 Nahar S N and Pradhan A K 2016 *Phys. Rev. Lett.* **117** 249502
[26] Pradhan A K and Nahar S N 2018 *ASP Conf. Ser* vol 515 p 79
[27] Nahar S N 2018 *Norad: Nahar-OSU-Radiative-Atomic-Data* (The Ohio State University) (available at: http://norad.astronomy.osu.edu)
[28] TOPbase 2018 (available at: https://cdsweb.u-strasbg.fr/topbase/topbase.html)
[29] The Rosseland mean is analogous to the effective resistance of parallel resistors in an electric circuit given by the harmonic mean 1/R; total atomic absorption at each frequency ν determines the radiation that flows through. It follows that if the *minima* or windows in opacity are of enormous importance, and uncertainties therein may influence the RMO more than the peaks in the opacity spectrum
[30] We note in passing that the central temperature and the neutrino flux due to the dominant nuclear *pp* fusion reactions also depends on solar opacity which determines the radiation flux emitted through the photosphere
[31] Buldgen G, Eggenberger P, Noels A, Scuffair R, Amarsi A M, Grevesse N and Salmon S 2023 *Astron. Astrophys.* **669** L9
[32] Christensen-Dalsgaard J, Gough D O and Thompson M J 1991 *Astrophys. J.* **378** 413
[33] Basu S and Antia H M 1997 *Mon. Not. R. Astron. Soc.* **287** 189
[34] 2003 *The Opacity Project Data Version 3.3 Created by M.J* (Seaton)
[35] Oxygen opacity stems mainly from fully ionized or H-like O VIII and therefore unlikely to change because of the accuracy of atomic data
[36] Badnell N R and Seaton M J 2003 *J. Phys. B: At. Mol. Opt. Phys.* **36** 4367
[37] Atomic Spectra Database National Institute for Standards and Technology (available at: www.nist.gov)
[38] Berrington K A, Eissner W and Norrington P N 1995 *Comput. Phys. Commun.* **92** 290
[39] The BPRM codes used in the present RMOP calculations may be made available to interested collaborators
[40] Pradhan A K and Zhang H L 1997 *J. Phys. B: At. Mol. Opt. Phys.* **30** L571
[41] Nahar S N and Pradhan A K 1992 *Phys. Rev. Lett.* **68** 1488
[42] Seaton M J 1990 *J. Phys. B: At. Mol. Opt. Phys.* **23** 3255 see also other papers in [3]